

Engineering the work function of solution-processed electrodes of silver nanocrystal thin film through surface chemistry modification

Cite as: APL Mater. 6, 121105 (2018); <https://doi.org/10.1063/1.5066040>

Submitted: 12 October 2018 . Accepted: 21 November 2018 . Published Online: 13 December 2018

Mingi Seong, Haneun Kim , Seung-Wook Lee, Donghun Kim, and Soong Ju Oh



View Online



Export Citation



CrossMark

ARTICLES YOU MAY BE INTERESTED IN

Partially replacing Pb^{2+} by Mn^{2+} in hybrid metal halide perovskites: Structural and electronic properties

APL Materials 6, 121106 (2018); <https://doi.org/10.1063/1.5060953>

Research Update: Beyond graphene—Synthesis of functionalized quantum dots of 2D materials and their applications

APL Materials 6, 120701 (2018); <https://doi.org/10.1063/1.5067250>

Enhanced piezoelectric performance of the ZnO/AlN stacked nanofilm nanogenerator grown by atomic layer deposition

APL Materials 6, 121109 (2018); <https://doi.org/10.1063/1.5057889>



Measure Ready
M91 FastHall™ Controller

A revolutionary new instrument
for complete Hall analysis

Lake Shore
CRYOTRONICS



Engineering the work function of solution-processed electrodes of silver nanocrystal thin film through surface chemistry modification

Mingi Seong,^{1,a} Haneun Kim,^{1,a} Seung-Wook Lee,^{2,a} Donghun Kim,^{3,b} and Soong Ju Oh^{1,b}

¹Department of Materials Science and Engineering, Korea University, Seoul 02841, South Korea

²Department of Semiconductor Systems Engineering, Korea University, Seoul 02841, South Korea

³Computational Science Research Center, Korea Institute of Science and Technology, 5, Hwarang-ro 14-gil, Seongbuk-gu, Seoul 02792, South Korea

(Received 12 October 2018; accepted 21 November 2018; published online 13 December 2018)

A solution-processable electrode is a key component in flexible electronics. Despite recent studies on silver nanocrystal (Ag NC)-based electrodes with high conductivity, the absence of a strategy to control the work function has limited the development of low-cost and high-performance electronic devices. In this report, we introduce a chemical route to manipulate the work function of solution-processed Ag NC-based electrodes. The structural, chemical, optical, and electronic properties, as well as the work functions, of the Ag NC thin films treated with three types of halide ligands (Cl^- , Br^- , and I^-) were investigated. Ultraviolet photoelectron spectroscopy analysis shows that the work functions are shifted to 4.76, 4.43, and 4.04 eV when the ligands are changed to Cl^- , Br^- , and I^- , respectively. The trend in the shift induced by the halide ligands matches the results of atomistic density functional theory calculations and scales with the strength of the dipoles formed by the electron transfer at the NC/ligand interfaces. To demonstrate the impact of our strategy in device applications, we fabricated all-NC-based thin-film transistors and complementary metal-oxide-semiconductor inverters. This study provides a fundamental understanding of the surface states of nanomaterials and also offers technological benefits for the construction of low-cost, high-performance electronic devices. © 2018 Author(s). All article content, except where otherwise noted, is licensed under a Creative Commons Attribution (CC BY) license (<http://creativecommons.org/licenses/by/4.0/>). <https://doi.org/10.1063/1.5066040>

A solution-processable metal electrode has gained huge attention in flexible electronic devices,^{1–7} because of the simple, low-cost fabrications as well as the compatibility with large-area substrates.^{8–14} Out of many metal candidates, silver nanocrystal (Ag NC) is a promising one as they are relatively inexpensive, highly conductive, and easily synthesized at a large scale. However, as-synthesized Ag NC thin films are electrically insulating because Ag NCs are surrounded by insulating organic ligands or surfactants for colloidal stability. Therefore, extensive efforts have been devoted to improving the electrical conductivity of thin films made of Ag NCs by various methods.^{15–22} Through these processes, highly conductive Ag NC thin films have been produced.

Beside the conductivity, the work-function of a metal is another critical property to be considered when used as an electrode because it determines the band alignments and barrier heights for charge injections or extractions. In conventional electrodes, different types of metals are used for controlling work functions of electrodes. For instance, Al is used for low work function contacts (4.1–4.2 eV),

^aM. Seong, H. Kim, and S.-W. Lee contributed equally to this work.

^bElectronic addresses: donghun@kist.re.kr and sjoh1982@korea.ac.kr

and Au is used for high work function electrodes (5.1–5.4 eV).²³ On the other hand, for solution processed electrodes, material selection is limited; for Al NCs, it is difficult to synthesize due to surface oxidation issues; for Au NCs, it is very expensive and difficult to obtain a conductive thin film as Au has higher melting temperature and less mobile and diffusive nature, compared to Ag. This restricts the range of work functions, severely limiting device applications. In this regard, the strategy to control the work function of solution-processed electrodes of Ag NCs should be urgently developed.

Here, we developed a chemical route to engineer the work function of Ag-NC-based electrodes through ligand exchange processes. We used short inorganic halide ligands for ligand exchange with the original long oleic acid ligands.^{24–26} The effects of different halide ions on the electronic, structural, chemical, optical properties, and more importantly the work function of Ag NC thin films were thoroughly investigated. Along with our combined analysis, density functional theory (DFT) calculations show that the origin of the work function change is the dipoles formed around the Ag NCs by the halide ions. Utilizing the developed method of halide-ion exchange, we fabricated all-solution-processed NC thin film transistors and complementary metal-oxide-semiconductor (CMOS) inverters with work-function-variable Ag NC electrodes to demonstrate their potential applications in flexible electronics. Our strategy provides a promising route to construct low-cost and high-performance electronics and optoelectronics.

The Ag NCs were synthesized by a simple solution process.²⁷ The synthesized Ag NCs have a spherical shape with uniform size (3–4 nm), as shown in Fig. 1(a), and are capped by long carbon chains of oleylamine and oleic acids. The as-synthesized Ag NC thin film cannot be used as an electrode because the interparticle distance is large and the thin film is electrically insulating. Therefore, we replaced these long organic ligands with halide ions to achieve high conductivity by a ligand exchange method. As the ligand exchange materials, solutions of ammonium chloride (NH₄Cl), tetrabutylammonium bromide (TBAB), and tetrabutylammonium iodide (TBAI) were prepared with the concentration of 30×10^{-3} M in methanol. The deposited Ag NC thin film was immersed in the prepared solution. After ligand treatment with halide ions for 2 min, the Ag NC thin film was washed three times with methanol to remove the residual ligands. This method was repeated 2–3 times to fill any cracks or holes.²⁸

To investigate the surface chemistry and optical properties of the Ag NC thin films treated with NH₄Cl, TBAB, and TBAI, Fourier transform infrared (FT-IR) spectroscopy measurement was

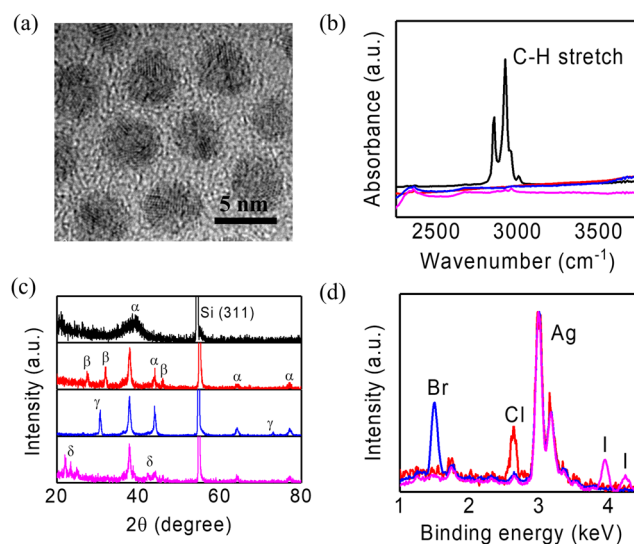


FIG. 1. (a) Transmission electron microscopy image of as-synthesized Ag NCs. (b) FT-IR spectra, (c) X-ray diffraction pattern, and (d) energy dispersive X-ray spectra of as-synthesized Ag NCs and NH₄Cl, TBAB, and TBAI-treated Ag NCs (black: untreated Ag NCs, red: NH₄Cl-treated Ag NCs, blue: TBAB-treated Ag NCs, and magenta: TBAI-treated Ag NCs; the peaks marked α , β , γ , and δ are attributed to crystalline Ag, AgCl, AgBr, and AgI, respectively).

conducted. As shown in the FT-IR spectra in Fig. 1(b), the as-synthesized Ag NCs yield intense peaks at 2922 and 2855 cm^{-1} , corresponding to the C–H stretching vibrations of oleate.²⁹ After ligand exchange, the corresponding peaks disappeared, indicating the removal of oleate.^{30,31}

We also investigated the structural properties of the Ag NC thin film through X-ray diffraction (XRD) analysis, as shown in Fig. 1(c). In the case of the as-synthesized Ag NC thin film, there is a broad peak at 38° that corresponds to the Ag face-centered-cubic (FCC) (111) plane. After ligand exchange, peaks near 38.08° , 44.32° , 64.52° , and 77.4° appeared, corresponding to the (111), (200), (220), and (311) planes of Ag. The peaks were more intense and sharper, implying the growth of the Ag NCs into larger crystals.³² Additional peaks also appeared, and these correspond to silver halides. In the case of NH_4Cl treatment, peaks were observed near 27.82° , 32.14° , and 46.26° , corresponding to the (111), (200), and (220) planes of AgCl. In the case of TBAB treatment, peaks were observed near 30.86° and 73.26° , corresponding to the (200) and (420) planes of AgBr. In the case of TBAI treatment, peaks corresponding to the (100), (002), (101), (110), and (112) facets of $\beta\text{-AgI}$ appeared near 22.09° , 23.40° , 24.98° , 38.72° , and 42.30° . The strong and sharp peak observed at around 55° is attributed to the silicon substrate. Thus, combined analysis confirms that the ligand exchange process with NH_4Cl , TBAB, and TBAI successfully replaced the oleate ligands with halide ions (Cl^- , Br^- , and I^- , respectively).

To study the surface states, quantitative and qualitative elemental analysis was carried out using energy dispersive X-ray spectroscopy (EDX). As shown in Fig. 1(d), there were peaks at 2.98/3.16, 2.62, 1.49, and 3.95/4.25 keV, corresponding to Ag, Cl, Br, and I, and the relative amounts of Cl^- , Br^- , and I^- ligands are 19.6%, 24.5%, and 27.2%, respectively. For further investigation, X-ray photoelectron spectroscopy (XPS) was also conducted and indicated that each ligand had successfully bound to Ag atoms (Fig. S1 in the supplementary material).

We examined the electronic properties of thin films after ligand exchange. Two-point resistance measurements were conducted with Cl^- , Br^- , and I^- -exchanged Ag NC thin films. As shown in Fig. 2(a), linear current–voltage (I – V) curves were obtained. The resistivity of as-synthesized Ag NC thin films is higher than our instrument limit of $2.00 \times 10^5 \Omega \text{ cm}$, due to long length of ligands and interparticle distances. The Cl^- - and Br^- -exchanged Ag NC thin films show similar high conductivities, whereas the I^- -exchanged Ag NC thin films show lower conductivities. The low conductivity of the I^- -exchanged Ag NC thin films is attributed to the larger ionic radius. The ionic radii of Cl^- , Br^- , and I^- are 0.181, 0.196, and 0.220 nm, respectively, increasing with the period number. The larger ionic radius creates slightly longer interparticle distances, weakening the NC coupling.^{23,33} Considering the thickness of the thin films, the resistivity is calculated as $(4.71 \pm 0.14) \times 10^{-5} \Omega \text{ cm}$

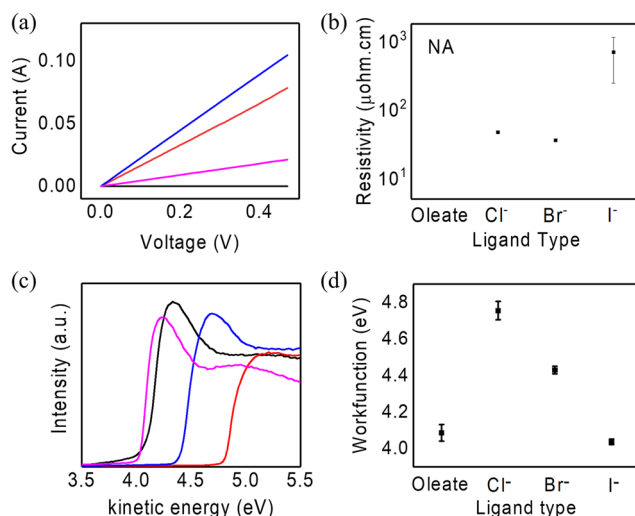


FIG. 2. Electrical properties: (a) current–voltage (I – V) curve and (b) resistivity of halide ligands treated Ag NCs. (c) Ultraviolet photoelectron spectroscopy plot (black: untreated Ag NCs, red: NH_4Cl -treated Ag NCs, blue: TBAB-treated Ag NCs, and magenta: TBAI-treated Ag NCs) and (d) calculated work function of the halide-treated Ag NCs.

for the Cl^- -exchanged thin film, $(3.59 \pm 0.14) \times 10^{-5} \Omega \text{ cm}$ for the Br^- -exchanged thin film, and $(6.94 \pm 6.86) \times 10^{-4} \Omega \text{ cm}$ for the I^- -exchanged thin film [Fig. 2(b)].

To investigate the work function of Ag NC thin films treated with various halide ions, ultraviolet photoelectron spectroscopy (UPS) analysis was performed, as shown in Fig. 2(c). The work function is the minimum thermodynamic energy needed to remove an electron from the solid to the vacuum state. In UPS measurements, when the incident photon energy becomes larger than the binding energy, bound electrons are freed and collected. The work function was then calculated by extrapolating to the intersection of the x -axis of the tangent line of the UPS spectrum. The work function was $4.09 \pm 0.04 \text{ eV}$ in the case of the as-synthesized Ag NCs, and it changed to 4.76 ± 0.05 , 4.43 ± 0.02 , and $4.04 \pm 0.01 \text{ eV}$ after ligand exchange with Cl^- , Br^- , and I^- , respectively, as shown in Fig. 2(d). The work function and spectra shift to higher voltages in the order of I^- , Br^- , and Cl^- , indicating that the binding energy is in the same order. We found that the ligand exchange process dramatically changed the work function of the NC thin films, as well as increased the conductivity. As 0-D NCs are materials having the high surface-to-volume ratio and the ligands directly affect the surface of NCs, the electronic structures and properties can be finely controlled with this ligand engineering strategy.

DFT calculations were performed to investigate the origin of the change in the work function. The surface of the Ag NCs was modeled as a semi-infinite Ag (111) slab geometry, as shown in Fig. 3(a), because the (111) surfaces are known to be dominantly exposed for Ag NCs. Modeling the NC surface as a slab is much more computationally efficient than modeling the entire NC, and the qualitative description of the electrostatic environment at NC/ligand interfaces should be similar in both cases. Only one side of the Ag slab was ligand-passivated. Four ligands (formate, Cl^- , Br^- , and I^-) were tested, with the ligand coverage held constant at one ligand per four surface Ag atoms. The formate in the simulation represents the oleate used in the actual experiments because the anchoring groups of these two ligands are chemically identical, and the ligands only differ in length.

Figure 3(b) shows the plane-averaged electrostatic potentials for the four ligands adsorbed onto Ag (111) slabs. A particular attention should be given to the flat potential lines in the vacuum region right across the ligands: different ligands lead to different vacuum energy shifts (ΔE_{vac}). The vacuum energy shift directly signifies the work function shift of the metal, in the opposing direction. ΔE_{vac} is the largest (+1.10 eV) for Cl^- , followed by +0.93 eV for Br^- , +0.78 for formate, and +0.53 eV for I^- . The direction and ordering of ΔE_{vac} agree well with the UPS results although the magnitude of the shifts is slightly overestimated by DFT.

ΔE_{vac} upon ligand passivation can usually be decomposed into two dipole terms: (1) a contribution from the dipole formed by the electron transfer at the NC/ligand interface and (2) a contribution from the intrinsic dipole of the ligand itself.^{34,35} Halide ions (Cl^- , Br^- , and I^-) lack an intrinsic dipole, and thus, ΔE_{vac} for halide ions only has an interfacial dipole term. Figure 3(c) shows the plane-averaged electron transfer for these three halide ligands. Electron transfer occurs from the Ag slabs to the ligands, and as a result the dipole points from the ligand to the Ag slab. The magnitude of the electron transfer, however, is distinctly different: it is largest for Cl^- , followed by those of Br^- and I^- , which is in agreement with the order of electronegativity of these elements (3.16 for Cl, 2.96

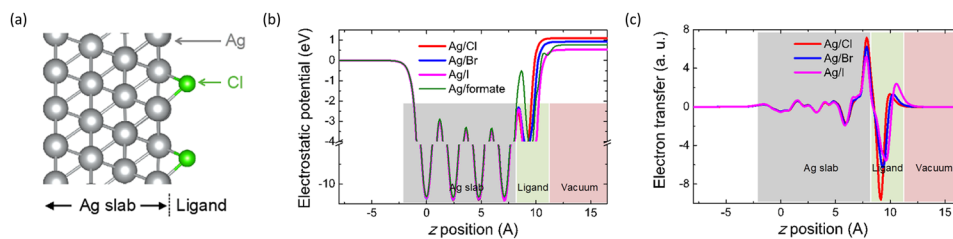


FIG. 3. DFT calculations of the ligand-induced vacuum energy shifts for Ag slabs. (a) Schematic diagram of the modeled Ag slab. Only the right side of the slab is passivated by adsorbed ligands (Cl^- ions are shown as an example). The ligand density was set at one ligand per four surface Ag atoms. (b) Plane-averaged electrostatic potentials of Ag slabs with different ligands. The potential in the vacuum region far to the left of the unpassivated Ag slab is set as zero. (c) Plane-averaged electron transfers of Ag slabs with different halide ligands.

for Br, and 2.66 for I on the Pauling scale). It is also noted that the work function of carboxylate cases (oleate in UPS and formate in DFT) is positioned between iodine and chlorine cases. In contrast to halogen ion cases where the intrinsic ligand dipole is non-existent, both the interface dipole and intrinsic dipole contribute to work function determination for carboxylate cases. Our simulation reveals that the interface dipole is positive and large for the formate ligand; however, it is weakened by the dipole of formate itself formed in the opposite direction. As a result, the net dipole of carboxylate becomes small and similar to the iodine case.

Advanced electronic circuits or devices require many fabrication steps and various materials because they require low work function materials (Al or Ag) for the n-type contacts but high work function materials (Au or Pt) for the p-type contacts. To overcome this limitation, we suggest Ag NC thin films treated with different halides as a work-function-variable electrode platform for electronic devices. As a proof of concept, we demonstrate n-type and p-type NC thin film transistor (TFT) and CMOS inverters using ambipolar materials of NH_4SCN -treated PbSe NCs. The PbSe NC thin film was formed on the patterned substrate by spin-coating, and ligand exchange with SCN^- was conducted. Br^- - and Cl^- -exchanged Ag NC thin films were used as the electrodes because they show much higher conductance compared to the I^- -exchanged Ag NC thin films, and they have different work functions, both of which are located in the band gap of the PbSe NCs. As shown in Fig. 4(a), the Br^- -exchanged Ag NC thin film electrode has a work function of 4.43 eV, which is higher than a Fermi level of the SCN^- -exchanged PbSe NC thin film. In this case, the transistor shows a high electron current and a low hole current, a signature of ambipolar n-type devices, as shown in Fig. 4(b). At the interface between the electrode and the PbSe NC channel, the barrier height for electrons is low, allowing easier electron injection. In the case of Cl^- -exchanged Ag NC thin film electrode, the work function is 4.76 eV, which is lower than the Fermi level of the SCN^- -exchanged PbSe NC thin films. The device has a high hole current and a low electron current, indicating that it is an ambipolar p-type device. Because the barrier height for holes is low, more hole injection is possible; thus, it becomes an ambipolar p-type channel, as shown in Fig. 4(c).

In addition, the CMOS inverter was fabricated by incorporating two types of transistors, having Ag NC thin film electrodes treated with NH_4Cl and TBAB.^{23,36} As shown in Fig. 4(d), an output voltage connected to each electrode of both transistors was generated by applying a drain voltage, and it was switched off by applying the gate voltage to the p-doped Si wafer. By using the first-order differential of the $V_{\text{in}} - V_{\text{out}}$ curve, the gate voltage at the switching point was found to be 20 V, and

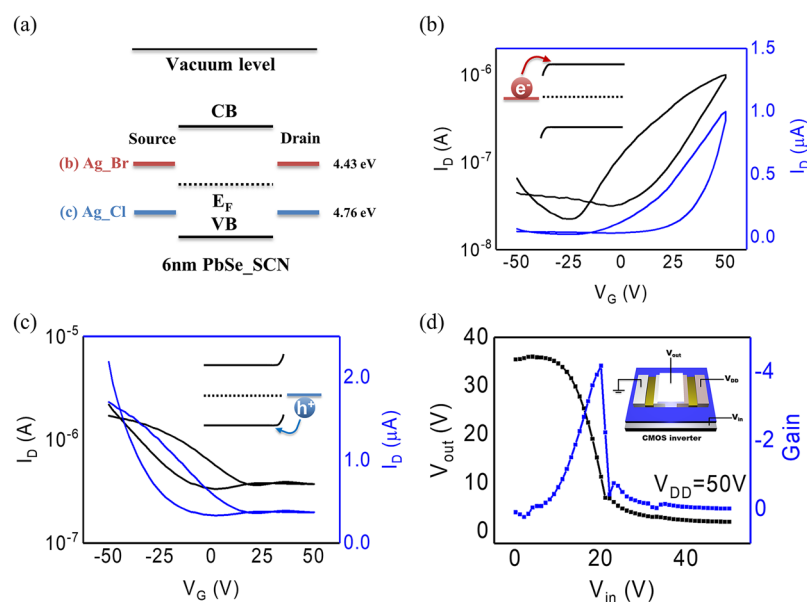


FIG. 4. (a) Schematic of the band structure in PbSe NC transistor. Transfer curves of field-effect transistors (FETs) with (b) TBAB-treated and (c) NH_4Cl -treated Ag NC electrodes. (d) Voltage transfer characteristic of the fabricated CMOS inverter.

the maximum gain was 4.17. Thus, the CMOS inverter was fabricated simply and inexpensively using a solution process, and we have shown that a single material comprising PbSe NCs can show both ambipolar n-type and p-type polarity when in contact with different halide-treated Ag NC electrodes. Because the metal work function determines the amount of charge injection,^{23,35} the conduction type of the device can be modified. Using only solution processes, we have demonstrated that NC building blocks can be combined to construct basic circuitry components.

We have introduced a simple solution-based method to achieve work-function-tunable electrodes using a ligand exchange process. Because the properties of the NCs are governed by their surface properties, the work functions of the NC thin films can be successfully modified in the range of 4.0–4.8 eV through halide ligand treatment. DFT and the characterization results show that the origin of the shift in the work function is the dipole formed at the surface between Ag and the ligands. Taking advantage of our simple methods, we have demonstrated ambipolar p-type and n-type all-nanocrystal transistors with high and low work functions, respectively, and prepared a CMOS inverter. The tunability of the work functions of solution processed electrodes provides an opportunity to design various electronic and optoelectronic devices.

See [supplementary material](#) for experimental details and XPS data of Ag NC thin films.

This research was supported by LG Innotek Co. Ltd (No. Q1715551). This was also supported by the Basic Science Research Program through the National Research Foundation of Korea (NRF) funded by Ministry of Science, ICT and Future Planning (No. 2016R1C1B2006534), the Creative Materials Discovery Program through the National Research Foundation of Korea (NRF) funded by the Ministry of Science and ICT (No. NRF-2018M3D1A1059001), the Korea University Future Research Grant, and the KIST institutional project (No. 2E28000).

- ¹ S. Yao and Y. Zhu, *Nanoscale* **6**, 2345 (2014).
- ² J. A. Rogers, T. Someya, and Y. Huang, *Science* **327**, 1603 (2010).
- ³ L. D. Deformable, S. Park, Y. Xiong, R. Kim, P. Elvikis, M. Meitl, D. Kim, J. Wu, J. Yoon, C. Yu, Z. Liu, Y. Huang, K. Hwang, P. Ferreira, X. Li, K. Choquette, and J. A. Rogers, *Science* **325**, 977 (2009).
- ⁴ J. Viventi, D. H. Kim, L. Vigeland, E. S. Frechette, J. A. Blanco, Y. S. Kim, A. E. Avrin, V. R. Tiruvadi, S. W. Hwang, A. C. Vanleer, D. F. Wulsin, K. Davis, C. E. Gelber, L. Palmer, J. Van Der Spiegel, J. Wu, J. Xiao, Y. Huang, D. Contreras, J. A. Rogers, and B. Litt, *Nat. Neurosci.* **14**, 1599 (2011).
- ⁵ B. Y. Ahn, E. B. Duoss, M. J. Motala, X. Guo, S. Park, J. Yoon, R. G. Nuzzo, J. A. Rogers, and J. A. Lewis, *Science* **323**, 1590 (2009).
- ⁶ M. Kaltenbrunner, T. Sekitani, J. Reeder, T. Yokota, K. Kuribara, T. Tokuhara, M. Drack, R. Schwödiauer, I. Graz, S. Bauer-Gogonea, S. Bauer, and T. Someya, *Nature* **499**, 458 (2013).
- ⁷ T. Someya, Z. Bao, and G. G. Malliaras, *Nature* **540**, 379 (2016).
- ⁸ Y. Xia, K. Sun, and J. Ouyang, *Adv. Mater.* **24**, 2436 (2012).
- ⁹ S. Kee, N. Kim, B. Park, B. S. Kim, S. Hong, J. H. Lee, S. Jeong, A. Kim, S. Y. Jang, and K. Lee, *Adv. Mater.* **30**, 1703437 (2018).
- ¹⁰ E. Lee, J. Ahn, H. C. Kwon, S. Ma, K. Kim, S. Yun, and J. Moon, *Adv. Energy Mater.* **8**, 1702182 (2017).
- ¹¹ J. Du, S. Pei, L. Ma, and H. M. Cheng, *Adv. Mater.* **26**, 1958 (2014).
- ¹² T. Someya, T. Sekitani, S. Iba, Y. Kato, H. Kawaguchi, and T. Sakurai, *Proc. Natl. Acad. Sci. U. S. A.* **101**, 9966 (2004).
- ¹³ Y. J. Choi, J. S. Kim, J. Y. Cho, H. J. Woo, J. Yang, Y. J. Song, M. S. Kang, J. T. Han, and J. H. Cho, *Chem. Mater.* **30**, 636 (2018).
- ¹⁴ E. Polydorou, A. Soultati, and M. Vasilopoulou, *J. Mater. Chem. C* **4**, 691 (2016).
- ¹⁵ K.-S. Moon, H. Dong, R. Maric, S. Pothukuchi, A. Hunt, Y. Li, and C. P. Wong, *J. Electron. Mater.* **34**, 168 (2005).
- ¹⁶ P. Laakso, S. Ruotsalainen, E. Halonen, M. Mantysalo, and A. Kemppainen, *ICALEO* **205**, 1360 (2009).
- ¹⁷ M. Bolduc, C. Trudeau, P. Beaupré, S. G. Cloutier, and P. Galarneau, *Sci. Rep.* **8**, 1418 (2018).
- ¹⁸ S. Ma, V. Bromberg, L. Liu, F. D. Egitto, P. R. Chiarot, and T. J. Singler, *Appl. Surf. Sci.* **293**, 207 (2014).
- ¹⁹ S. Wünsch, S. Stumpf, A. Teichler, O. Pabst, J. Perelaer, E. Beckert, and U. S. Schubert, *J. Mater. Chem.* **22**, 24569 (2012).
- ²⁰ A. Albrecht, A. Rivadeneyra, A. Abdellah, P. Lugli, and J. F. Salmerón, *J. Mater. Chem. C* **4**, 3546 (2016).
- ²¹ J. Perelaer, M. Klokkenburg, C. E. Hendriks, and U. S. Schubert, *Adv. Mater.* **21**, 4830 (2009).
- ²² Z. Zhang and W. Zhu, *J. Alloys Compd.* **649**, 687 (2015).
- ²³ S. J. Oh, Z. Wang, N. E. Berry, J.-H. Choi, T. Zhao, E. A. Gaulding, T. Paik, Y. Lai, C. B. Murray, and C. R. Kagan, *Nano Lett.* **14**, 6210 (2014).
- ²⁴ S.-W. Lee, H. Joh, M. Seong, W. S. Lee, J.-H. Choi, and S. J. Oh, *J. Mater. Chem. C* **5**, 2442 (2017).
- ²⁵ D. Zhitomirsky, M. Furukawa, J. Tang, P. Stadler, S. Hoogland, O. Voznyy, H. Liu, and E. H. Sargent, *Adv. Mater.* **24**, 6181 (2012).
- ²⁶ Z. Ning, O. Voznyy, J. Pan, S. Hoogland, V. Adinolfi, J. Xu, M. Li, A. R. Kirmani, J. Sun, J. Minor, K. W. Kemp, H. Dong, L. Rollny, A. Labelle, G. Carey, B. Sutherland, I. Hill, A. Amassian, H. Liu, J. Tang, O. M. Bakr, and E. H. Sargent, *Nat. Mater.* **13**, 822 (2014).

- ²⁷ J. Park, S. G. Kwon, S. W. Jun, B. H. Kim, and T. Hyeon, *ChemPhysChem* **13**, 2540 (2012).
- ²⁸ M. A. Boles, D. Ling, T. Hyeon, and D. V. Talapin, *Nat. Mater.* **15**, 141 (2016).
- ²⁹ H. G. Bagaria, E. T. Ada, M. Shamsuzzoha, D. E. Nikles, and D. T. Johnson, *Langmuir* **22**, 7732 (2006).
- ³⁰ W. S. Lee, S.-W. Lee, H. Joh, M. Seong, H. Kim, M. S. Kang, K.-H. Cho, Y.-M. Sung, and S. J. Oh, *Small* **13**, 1702534 (2017).
- ³¹ H. Kim, S. W. Lee, H. Joh, M. Seong, W. S. Lee, M. S. Kang, J. B. Pyo, and S. J. Oh, *ACS Appl. Mater. Interfaces* **10**, 1389 (2018).
- ³² M. Seong, S. W. Lee, H. Joh, W. S. Lee, T. Paik, and S. J. Oh, *J. Alloys Compd.* **698**, 400 (2017).
- ³³ J. Wei, N. Schae, and M. Pileni, *J. Phys. Chem. B* **118**, 14070 (2014).
- ³⁴ S. Yang, D. Prendergast, and J. B. Neaton, *Nano Lett.* **12**, 383 (2012).
- ³⁵ P. R. Brown, D. Kim, R. R. Lunt, N. Zhao, M. G. Bawendi, J. C. Grossman, and V. Bulović, *ACS Nano* **8**, 5863 (2014).
- ³⁶ D. M. Sun, M. Y. Timmermans, Y. Tian, A. G. Nasibulin, E. I. Kauppinen, S. Kishimoto, T. Mizutani, and Y. Ohno, *Nat. Nanotechnol.* **6**, 156 (2011).